Analyst

Accepted Manuscript

This article can be cited before page numbers have been issued, to do this please use: R. Urteaga, E. Elizalde and C. L.A. Berli, *Analyst*, 2018, DOI: 10.1039/C8AN00149A.

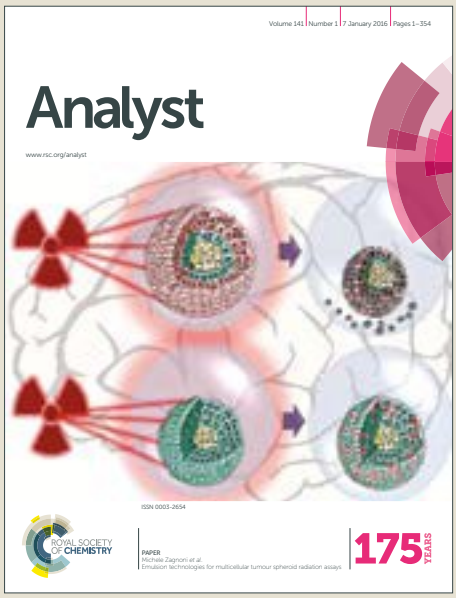

ROYAL SOCIETY OF CHEMISTRY

rsc.li/analyst

View Article Online
DOI: 10.1039/C8AN00149A

Journal Name

ARTICLE

Transverse solute dispersion in microfluidic paper-based analytical devices (µPADs)

Received 00th January 20xx,
Accepted 00th January 20xx

DOI: 10.1039/x0xx00000x

www.rsc.org/

Raúl Urteaga,[a] Emanuel Elizalde †[b] and Claudio L. A. Berli *[c]

The transport of molecules and particles across adjacent flow streams is a key process in several operations implemented in microfluidic paper-based analytical devices (µPADs). Here, the transverse dispersion of a analytes was quantitatively evaluated by theory and experiments. Different tests were carried out to independently measure the coefficients of both Brownian diffusion and mechanical dispersion under capillary-driven flow. The dispersion width was found to be independent of fluid velocity and analyte properties, and fully determined by the dispersivity coefficient, which is a characteristic of the paper microstructure. This information introduces a change of paradigm for the design of mixers, diluters, and concentration gradient generators on µPADs; therefore, efforts were addressed to rationalize these operations on paper. The research reveals that mixers and concentration gradient generators can be much more efficient than their counterparts made on conventional microchannels; in contrast, separators such as the H-filter need to be appropriately engineered on paper, because the working principle can be hindered by mechanical dispersion. The knowledge gained throughout this work would contribute to design µPADs with a new level of precision and control over the formation of localized concentration profiles.

Introduction

Several analytical and preparative operations implemented on microfluidic paper-based analytical devices (µPADs) exploit a common transport process: the transverse dispersion of molecules across adjacent flow streams. Operations such as mixing, dilution, separation, and extraction were demonstrated in a seminal work,[1] and afterward extended to a number of applications.[2-4] In particular, the generation of concentration gradients is of considerable interest in drug discovery, cell culture, and medical diagnostics.[5] Further, as cell culture[6] and chemotaxis studies[7] are being implemented on paper, the development of concentration gradient generators on the same substrate is a current need, and proposals are just emerging in the literature.[8,9] In this context, the aim of the present work is to investigate the foundations of transverse solute dispersion in paper, in order to improve the manipulation of localized concentration profiles in µPADs.

The physical basis of transverse dispersion in porous media are known since many years.[10] Early motivations were in the fields of geology,[11] chromatography,[12] and chemical engineering,[13] and the matter is regularly revisited in the literature.[14-16] Nevertheless, the implications of this knowledge in the development of µPADs have not been discussed yet. In fact, research in the field of paper-based microfluidics has been mostly focused on fabrication methods[17,18] and flow control,[19,20] and less attention has been paid to the transport of species. The few exceptions to be noted are works dealing with distance-based measurements,[21] the improvement of sample distribution in complex geometries,[22] and notably, the evaluation of the amount of analyte effectively transported by the flow.[23,24] Concerning transverse dispersion in substrate materials used to manufacture µPADs, no quantitative studies have been published up to date, to our knowledge. As an interesting exception, a study of mixing in strips made on clean room paper has been reported,[25] where effective diffusion coefficients larger than molecular diffusion coefficients were suggested to explain the resulting mixing performance.

The present work explores the problem of transverse solute dispersion by theory and experiments. Brownian diffusion and transverse mechanical dispersion were independently assessed for three different filter papers, chosen among those typically used in µPADs. A coefficient that characterizes dispersivity in each paper is reported here for the first time, which was deduced after appropriate data analysis in the framework of transport phenomena in porous media. The fact that mechanical dispersion is the dominant mechanism (for typical flow regimes on paper) introduces a paradigm shift in the rationalization of operations based on transverse dispersion. Therefore, the insights gained on the subject are addressed to improve the design of specific operations

[a] IFIS-Litoral (Universidad Nacional del Litoral-CONICET), Güemes 3450, 3000, Santa Fe, Argentina.
[b] INTEC (Universidad Nacional del Litoral-CONICET), Predio CCT-CONICET, RN 168, 3000, Santa Fe, Argentina.
† Present address: LFD, Facultad de Ingeniería, UBA, CABA, Argentina.
* Corresponding author. E-mail address: cberli@santafe-conicet.gov.ar
Electronic Supplementary Information (ESI) available: [details of any supplementary information available should be included here]. See DOI:10.1039/x0xx00000x

View Article Online
DOI: 10.1039/C8AN00149A

implemented in μPADs: concentration gradient generators, mixers, and diffusion-based separators.

Theory

The basic problem to consider is stated in Fig. 1a: a porous substrate with co-flows of average velocity v_L in *y*-direction. One of the flow streams transports a dye constituted by molecular species or small particles, which are advected by the flow and dispersed by Brownian motion. In the pore space, the alternating variation of fluid velocity, in both magnitude and direction, introduces an additional dispersion. This mechanical effect is normally characterized by coefficients that independently measure the longitudinal (D_L) and the transverse (D_T) dispersivities. This work is hereafter focused on dispersion transverse to the flow, i.e. in the *x*-direction of

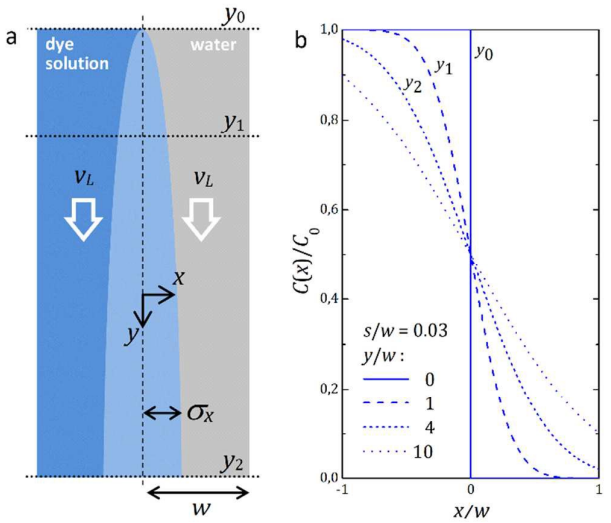

Fig. 1. (**a**) Drawing of a steady co-flow of dye solution and pure water in a paper strip. (**b**) Transverse concentration profiles of the dye along the flow path, according to the prediction of eqn (3). Full, dashed, and short-dashed lines correspond to the transects indicated in Fig. 1a. The dotted line corresponds to the downstream distance where dye concentration is around 10 % of C_0 at $x = w$.

Fig. 1a.

A common formulation for the transverse dispersion coefficient is[10,14,16]

$$D_T = D_0 + sv_L, \qquad (1)$$

where D_0 is the molecular diffusion coefficient and s is the dispersivity constant. In eqn (1), the second term represents the mechanical dispersion that linearly increases with fluid velocity. When $v_L \to 0$, $D_T \to D_0$, as molecular diffusion is always active. On the other hand, for relatively large v_L, $D_T \gg D_0$, which means that mechanical dispersion is the dominant mechanism in the pore space. In this regime, the dispersion coefficient can be interpreted as follows: $D_T = \langle \Delta x^2 \rangle / \Delta t = sv_L$, where the second equality takes into account that $v_L = \langle \Delta y \rangle / \Delta t$, and hence $s \equiv \langle \Delta x^2 \rangle / \langle \Delta y \rangle$. The dispersivity constant s accounts for the lateral dispersion of solute and, at the same time, represents a characteristic dimension of the porous matrix, being on the order of pore length or distance between junctions. The transition from one regime (pure molecular diffusion) to the other (mechanical dispersion) occurs around a critical fluid velocity $v_{L,c} = D_0/s$.[14] The coefficient D_0 can be determined by measuring the steady state concentration profile of a given tracer in a system of two parallel flow streams, one of them initially with zero concentration (Fig. 1a). For uniform v_L, the concentration profile $C(x, y)$ is governed by Fick's second law[10] with the change of variable $t = y/v_L$. The solution of the governing equation for the right initial $[C(x < 0) = C_0, C(x > 0) = 0]$ and boundary conditions $[C(x \to -\infty) = C_0, C(x \to \infty) = 0]$ is[26]

$$\frac{C(x,y)}{C_0} = \frac{1}{2}\mathrm{erfc}\left[\frac{x}{2(D_T y/v_L)^{1/2}}\right]. \qquad (2)$$

where $\mathrm{erfc}[z]$ is the complementary error function defined as follows: $\mathrm{erfc}[z] = (2/\sqrt{\pi}) \int_z^\infty e^{u^2} du$; $z = x/(2(D_T y/v_L)^{1/2})$. Equation (2) implies that the time-evolution of $C(x)$ can be captured at each transect $y = v_L t$ along the flow path, as represented in Fig. 1b. Furthermore, in operation conditions where molecular diffusion can be neglected in front of transverse dispersion, $D_T \approx sv_L$, and eqn (2) simplifies to

$$\frac{C(x,y)}{C_0} = \frac{1}{2}\mathrm{erfc}\left[\frac{x}{2(sy)^{1/2}}\right]. \qquad (3)$$

The relevant meaning of this equation is that the variance $\sigma_x^2 = D_T t = sy$ results linearly proportional to the downstream distance y by the dispersivity constant s. Therefore, in this flow regime ($v_L > v_{L,c}$), the dispersion width $\sigma_x = (sy)^{1/2}$ expected in a paper-based device is independent of fluid velocity and dye properties, and fully determined by the paper microstructure.

In order to test these predictions, experiments planned to explore both the conditions under which $D_T \gg D_0$ and the linear relation $D_T \approx sv_L$. For the measurement of D_T, the problem posed in Fig. 1a was implemented in practice (see Fig. 2a below), where flow is driven by capillary action, and hence different fluid velocities were achieved by using different strip lengths. For the independent measurement of D_0, a different configuration was necessary to clearly set up the initial conditions. A paper strip with inlet ports at both ends was used (see Fig. 2c below), which were simultaneously filled with pure water and dye solution, respectively. Capillary-driven flows developed in opposite directions. When fluid fronts met at the center of the strip, an arrested interface was formed with dye concentration satisfying a step-like function, which constituted the initial condition of the experiment. Then the evolution of the concentration profile was measured over time, the liquid being in quiescent conditions with controlled evaporation.

Experimental

Materials and methods

View Article Online
DOI: 10.1039/C8AN00149A

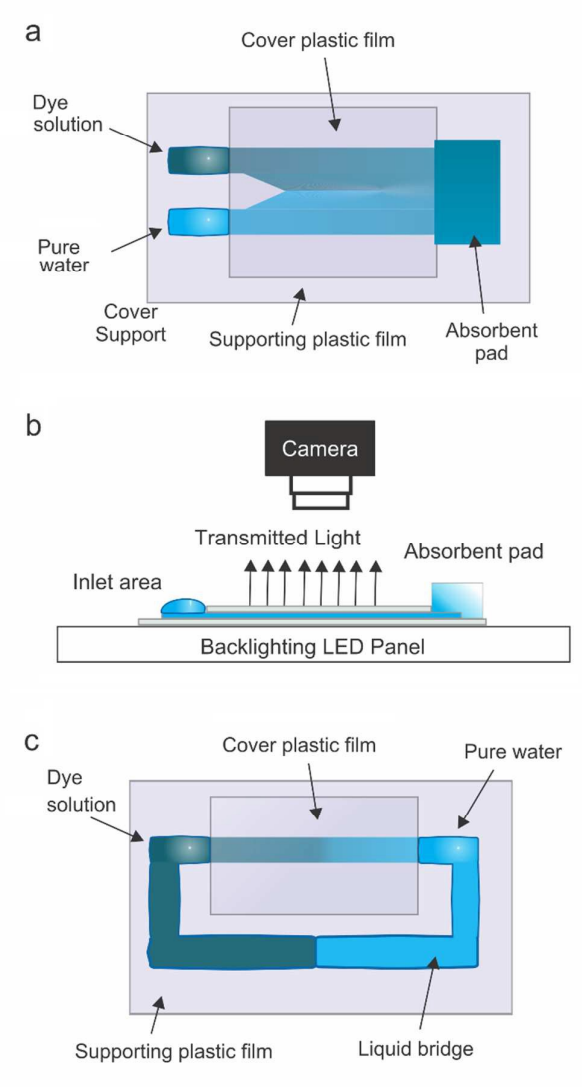

Fig. 2. Schematic representation of the setup used to measure the transverse dispersion coefficient in laminated paper strips. (**a**) Top view of the Y-shaped paper strip with a steady co-flow of pure water and dye solution. (**b**) Side view of the configuration used to capture the transmitted light as function of time during the dye dispersion experiments. (**c**) Top view of the uniform strip used to measure the molecular diffusion coefficient in arrested flow conditions; a bridge of wet paper was used to equalized the head pressure at inlet ports.

Paper-based devices were fabricated by craft-cutting and hot lamination.[27] Three different filter papers were used in the experiments: Whatman qualitative filter paper grade 1 (W1), Muntkell filter paper 00A (M), and Schleicher & Schuell 0859 filter paper (SS). In all cases, the main channel was 15 mm wide and the total length varied between 20 and 60 mm. The inlet arms of Y-shaped channels were 5 mm wide and 20 mm long. Paper channels were laminated in film pouches (150 µm thick) at 130 °C, at the speed of 3.5 mm/s. Previous to lamination, care was taken to avoid air gaps at the paper strip borders, as the resulting sharp edges may drag liquid along the channel. The effect can be diminished by using high temperature and pressure during lamination,[28] self-adhesive lamination sheets,[29] or selective heating around the paper edges.[30] Here, a fluorinated acrylics-based hydrophobic spray (Imper Ital Protect, Muntex SA, Munro, Argentina) was sprayed onto the films before lamination. The plastic film surfaces became hydrophobic and the air gap remained dry over the whole imbibition process. Perforations were made on the lamination films to form the inlet port in one end, and to connect the paper strip to an absorbent pad in the other end. The pad worked as a capillary pump to maintain a steady flow rate over the experiment. A hydro-soluble black dye (STA stamp ink, Fapyc SA, Buenos Aires, Argentina) was used as tracer in the main flow. In all tests, 2%(v/v) water solutions were used. Results reported here correspond to paper strips cut along the machine direction,[31] though no differences of statistical significance have been observed in the measured dispersion coefficients. All measurements were made at room temperature.

Transverse dispersion measurements

Paper strips with Y-shaped inlet arms (Fig. 2a) were employed to determine D_T. The dye dispersion was studied by measuring the optical absorbance (Fig. 2b), which enables a direct determination of dye concentration in real time. The device was horizontally placed over a white backlighting LED panel. Transmitted light was captures by using a high resolution digital camera (Canon EOS Rebel T5) connected to a PC. The camera was focused vertically at 20 cm over the device. The spatial resolution was about 22 µm/pixel and the frame rate was 12 frames/min. At the beginning of each experimental run, both inlet ports were filled with water. This step enabled to record the maximum of light transmittance. Once the paper strip was completely wet, one port was loaded with the dye solution. The flow completely stabilized after 50 min, approximately, and then the analysis of light absorbance was carried out. After each measurement, the strip was completely wet with the dye solution to record the minimum of light transmittance. These reference levels were then used to normalize intensity data. A script was implemented to analyze the images and extract the concentration profile (see data analysis below). The light intensity data were laterally averaged over a region of 20 pixels, which represents a distance of about 440 µm on the paper surface. The three RGB channels were averaged to obtain the final concentration profile.

Molecular diffusion measurements

A paper strip with inlet ports at both ends (Fig. 2c) was used to determine D_0. The manufactured device consists of a paper strip of 5 mm x 50 mm. In the lamination step, the paper strip was supported over one film and covered with a second one of 20 mm in length, in order to laminate the central region only, leaving the strip ends open to the atmosphere. The inlet ports were connected by a bridge of non-laminated paper, to ensure that the hydrostatic head is the same at strip ends. The ports were simultaneously filled with pure water and dye solution, respectively, thus capillary-driven flows developed in opposite

View Article Online
DOI: 10.1039/C8AN00149A
ARTICLE
Journal Name

directions. When fluid fronts met at the center of the strip, an arrested interface was formed ($v_L = 0$). The liquid at inlet ports was permanently replenished during the experiment. The time-evolution of light absorbance was followed by using the experimental setup described above (Fig. 2b), now employing a higher spatial resolution of about 15 µm on the paper surface; the frame rate was 1 frame/min.

Data analysis

Measured light intensity was related to ink concentration by a calibration procedure. The results of light transmittance with different ink dilutions are reported in Fig. 3b. For low ink concentrations, a linear relation between the ink content and light intensity was found, irrespective of the selected RGB camera channel. Fig. 3b shows that the linear region holds up to around 2%(v/v). This concentration value was chosen to maximize the image resolution. Thus, concentration profiles were obtained directly from light intensity data. An average over several pixels perpendicular to the concentration gradient was performed to define each data point, considering the information of all the RGB channels. In agreement with eqn (2), the image intensity profiles were fitted to the following expression: $a + b\ \mathrm{erfc}[(x - x_0)/2\sigma_x]$. The values of the fitting parameters a, b, and x_0 were used to normalize data, in order to represent the concentration profiles according to eqn (2). In particular, the time variation of the parameter $\sigma_x = (Dt)^{1/2}$ was then analyzed to extract the coefficient, either D_T or D_0, depending on the experiment.

Capillary filling measurements

The dynamic coefficient c of the capillary-driven flow was measured for the tested filter papers by using the experimental set up shown in Fig. 2b. In strips of uniform width, the infiltration rate is $v_L = dy/dt = c/y$, where $y(t)$ is the average fluid front position.[19] Thus c was obtained from simple infiltration experiments. Paper strips of 5 mm wide and 60 mm long were used. The inlet port was filled with pure water and the time evolution of the fluid front was optically followed (the change of light transmittance at the wetting front[31]). Data were analyzed according to $y(t) = (2ct)^{1/2}$, and c was determined as the fitting parameter. Values reported in Table 1 are the mean of at least 6 experiments.

Results

Molecular diffusion

Figure 3a presents two photographs showing the interface between pure water and dye solution, at the moment when fluid fronts get in contact and six hours later, respectively. The normalized concentration profile was obtained from optical absorbance, as described above. The average of about 80 pixels in the vertical direction was used to define each data point. Concentration data were then analyzed with the theoretical model (Fig. 3c). The fitting procedure, carried out over every picture recorded during measurement, yielded the parameter σ_x as a function of time. A linear analysis of σ_x^2 vs t allowed to determine $D_0 = 2.1(\pm 0.1)10^{-11}\ \mathrm{m}^2/\mathrm{s}$ (curve slope in Fig. 3d) for laminated W1 paper. It is worth noting that this value represents the effective diffusion coefficient in the paper fiber network, under stagnant flow conditions. Apart from determining D_0, this section provides valuable information on the prediction of the time-evolution of concentration profiles, which has practical interest as well; for example, the set up employed is useful to study cell chemotaxis on paper, with concentration gradient formed in situ.[8]

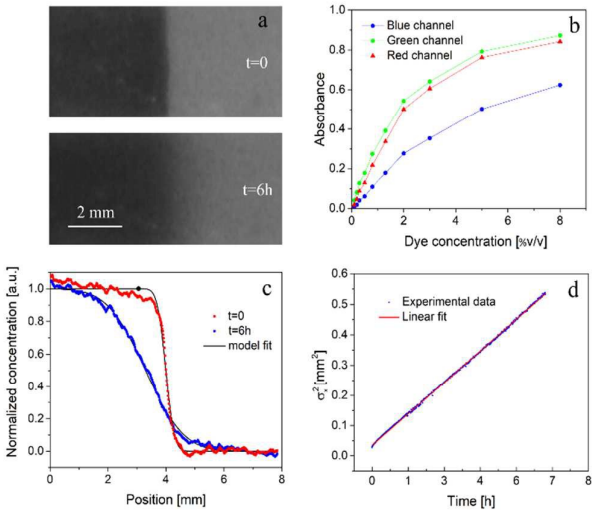

Fig. 3. (a) Photographs showing the pure water/dye solution interface in laminated W1 filter paper in stagnant flow conditions, just after the fluids get into contact and 6 hours later. **(b)** Light absorbance as a function of dye concentration for the different RGB camera channels **(c)** Normalized concentration profile obtained at the beginning of the experiment (red square symbols) and six hours later (blue circle symbols). Full lines are the numerical fitting with the theoretical model. **(d)** Temporal evolution of the variance σ_x^2 ; dots represent data from experiments and the full line is the linear fitting.

Transverse dispersion

Figure 4a presents a photograph of the Y-shaped paper device during an experimental run. Inlet ports were initially filled with pure water and, 25 s later, the right arm was loaded with the dye solution. The fluid velocity measured when the fluid front reached the absorbent pad was $v_L = 16$ µm/s. Once the stationary regime was attained, the dye concentration at each position was obtained from image analysis, as described above. Each data point contains the average information of 10 pixels. The residence time of a tracer particle in the paper strip can be calculated as $t = y/v_L$. The transverse concentration profiles at different downstream positions are reported in Fig. 4b. The fitting procedure with the theoretical model yielded data of σ_x as a function of time, from every position on the stationary image. Fig. 4c shows plots of σ_x^2 vs t. Data from experiments under flow are rather noisy in comparison to those in Fig. 3d. Nevertheless, given the large amount of data points, the slope of the curves (D_T) can be safely determined, and further averaged over different paper strips. The resulting mean value was $D_T = 5(\pm 0.6)\ 10^{-10}\ \mathrm{m}^2/\mathrm{s}$, for $v_L = 16\ \mu m/s$

View Article Online
DOI: 10.1039/C8AN00149A

in laminated W1 paper. This dispersion coefficient is about 25 times larger than the molecular diffusion coefficient D_0 determined above. Furthermore, as $D_T \gg D_0$ in the experiments, the dispersivity constant can calculated simply as $s = D_T/v_L = 30(\pm 4)\ \mu m$. Besides, the same experiment was made at a higher fluid velocity, by using a shorter paper strip. For $v_L = 58\ \mu m/s$, the result was $D_T = 1.6(\pm 0.2)\ 10^{-9}\ \mathrm{m^2/s}$. Now D_T is about 80 times higher than D_0, and $s = 28(\pm 5)\ \mu m$.

The fact that s remains unchanged in different flow regimes confirms the hypothesis made in the theoretical section: the coefficient D_T is linearly proportional to v_L and the dispersion width σ_x is independent v_L. The last outcome also ensures that potential variations of the fluid front do not affect the dispersion width, which entail remarkable advantages for the design of mixers and gradient generators, as described in next section.

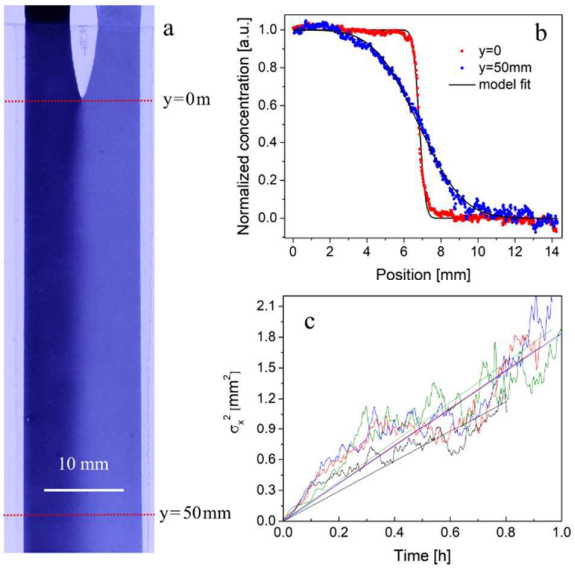

Fig. 4. (**a**) Photograph showing the streams of pure water and dye solution co-flowing at 16 µm/s in laminated W1 filter paper. (**b**) Normalized concentration profiles corresponding to the transects shown in Fig. 4a. Symbols represent the experimental values and lines are the theoretical model. (**c**) Temporal evolution of the parameter σ_x^2 for four different paper strips; lines are the best linear fitting in each case.

The experimental procedure illustrated in Fig. 4 was reproduced with laminated M and SS filter papers; at least four trials were made in each case. The results are summarized on Table 1 along with the nominal specifications of each filter paper. One may observe that s differs for each filter paper, which would be related to characteristic of fiber networks. In particular, the last column in Table 1 includes the dynamic coefficient c, which characterizes the capillary-driven flow of each paper ($v_L = c/y$ for uniform strips). In all cases, the reported error represents the standard deviation of measured data. Table 1 contains valuable information to handle transverse dispersion coupled to fluid dynamics in µPADS. Indeed, these are the first measured data of transverse dispersion in paper, to our best knowledge.

Table 1. Filter papers characteristics. Paper grammage, sheet thickness, and particle size retention are nominal specifications from manufacturers. The dispersivity *s* and dynamic coefficient *c* were measured in this work for laminated paper strips.

Paper	Grammage [g/m²]	Thickness [µm]	Retention [µm]	s [µm]	c [mm²/s]
W1	87	180	11	30±3	1.3±0.15
M	80	190	4-5	44±14	0.8±0.3
SS	61	140	7-12	38±13	1.4±0.15

One may further note that our results reasonably fall onto the master curves created with data from diverse porous materials,[10,14,15] which are customarily presented in plots of D_T/D_0 vs Pe, where $Pe = sv_L/D_0$ is the Péclet number at the pore level. For example, for laminated W1 paper, $D_T/D_0 = 25$ for $Pe = 23$, and $D_T/D_0 = 80$ for $Pe = 83$.

Design rules for basic operations on µPADS

Mixers and concentration gradient generators

In what follows we take advantage of the information gained on transverse dispersion to define the optimal geometries for basic operations. For capillary-driven flows in uniform strips ($v_L = c/y$), the condition $v_L > v_{L,c} = D_0/s$ is satisfied for distances shorter than $y_c = cs/D_0$. This critical distance is above 1 m for typical systems (from data in Table 1), thus eqn (3) can be safely applied in typical paper based-devices.

According to eqn (3), the dispersion width is related to the downstream distance y as $\sigma_x = (sy)^{1/2}$. Therefore, the only required parameter to design operations based on transverse solute dispersion is the dispersivity s. For example, if a concentration gradient transverse to a uniform strip is required across the full width $2w$, as illustrated in Fig. 5a, then the strip length l obeys to,

$$l = \frac{w^2}{4z_C^2 s}, \qquad (4)$$

where z_C is the argument of $\mathrm{erfc}[z_C]$ in eqn (3), a factor that specifies the desired species concentration C at $x = w$ and $y = l$. The concentration at the strip borders, $C(-w, l)$ and $C(w, l)$, can be chosen as 90 and 10% of C_0, respectively, which yields a practically linear gradient in the inner region (see the dotted line in Fig. 1b). According to eqn (3), this condition is satisfied when $z_C = 0.9$; therefore, the strip length required is $l \approx 0.3\, w^2/s$. As an example, for w = 1 mm in laminated W1 paper, $l \approx 10$ mm, i.e. $l/w \approx 10$. For w = 2 mm, l grows to 41 mm, given the nonlinear relation stated in eqn (4). It is worth noting that a pH gradient generator analogous to that in Fig. 5a has been lately reported;[32] the device was successfully used to deliver reactants to a highly localized precipitation reaction.

Alternatively, if the required design is for mixing two chemical species initially placed on different arms of the Y-shaped strip

View Article Online
DOI: 10.1039/C8AN00149A

(Fig. 5b), a certain mixing degree needs to be specified as target. For example, the concentration at the strip borders may be chosen as 60 and 40%, respectively, for a rather flat $C(x)$ distribution. Equation 3 predicts that $C(w,l)$ is 40% of C_0 when $z_C = 0.18$. Thus, for w = 1 mm in W1 paper, $l \approx 260$ mm, which is an impractical size for µPADs. However, if the width is w = 0.5 mm, l shortens to 66 mm.

Comparison to conventional (non-porous) microchannels

In mixers and gradient generators fabricated with conventional microchannels,[5] a tradeoff between diffusive and advective transports has to be made to define the channel length, because molecular diffusion is the only dispersive mechanism; the dispersion width in microchannels is $\sigma_{x,\mu ch} = (D_0 y/v_L)^{1/2}$, and decreases with fluid velocity. In contrast, the mechanism in paper is substantially different, since it is dominated by mechanical dispersion in the pore space; the dispersion width in paper channels is $\sigma_{x,paper} = (D_T y/v_L)^{1/2} = (sy)^{1/2}$. The lengths required in each system to attain the same dispersion width are related as follows, $l_{\mu ch}/l_{paper} = D_T/D_0 = sv_L/D_0$. This ratio reveals that the same gradient can be formed in a paper channel considerably shorter than a microchannel, taking into account that D_T/D_0 was measured to be in the range 20-100 for laminated filter paper. A remarkable consequence is that mixing can be achieved much more efficiently in µPADs than in conventional microchannels.

Concerning the generation of concentration gradients, paper enable the easy formation of a continuous and spatially distributed concentration profile on a single paper strip,[32] while conventional microfluidics requires a network of microchannels (typically with the tree-like format) to form discrete concentration profiles.[5] Moreover, the gradient formation on paper is entirely defined by the microstructural property of the fiber network, by means of the dispersivity s. According to eqn (4), the aspect ratio of the flow domain required for a given operation scales as $l/w \sim w/s$, which makes more evident that the dispersion width is independent on fluid velocity and particle characteristics. For these reasons, the design of mixers and diluters on paper requires strategies different than those used for conventional microchannels. Further relevant aspects are discussed in next sections.

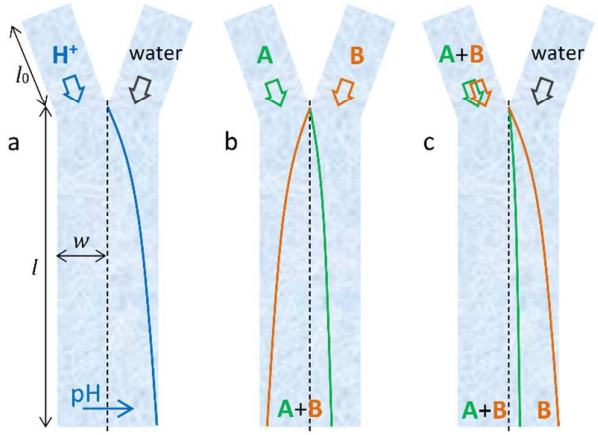

Fig. 5. Drawing of analytical operations based on transverse solute dispersion, where colored lines indicate the expansion of concentration profiles under flow. (**a**) Elementary concentration gradient generator: as a practical example, the dispersing species is hydrogen ion, which yield a pH gradient orthogonal to the flow. (**b**) Mixer: the species A and B injected in each stream interdiffuse to get mixed at the strip end. (**c**) Separator (H-filter): the species A and B, both injected in the left port, separate downstream due to dissimilar diffusivities.

Throughput and assay times

Maximizing the throughput of mixers and gradient generators is desirable for most applications. The goal can be achieved by parallelization, nonetheless it is useful to find the conditions that produce maximum flow rates or minimum assay times. For example, for the Y-shaped devices drawn in Fig. 5, when the fluid front reaches the position $y = l$, the flow rate is $Q = 2whv_L = 2whc/(l_0 + l)$,[19] where h is the paper thickness (Table 1) and l_0 is the length of inlet arms. Including the restriction of eqn (4), the flow rate results,

$$Q = \frac{2whc}{l_0 + w^2/(4z_C^2 s)}. \quad (5)$$

It is readily seen in eqn (5) that Q has a maximum when $l_0 \to 0$. If the hydrodynamic load of the inlet arms is effectively minimized, then the flow rate results $Q \approx 8hcz_C^2 s/w$. The first interesting result is that Q is inversely proportional to w. This apparently inconsistent relationship comes from the fact that the strip length l is constrained by eqn (4). Therefore, for gradient generators and mixers, minimizing the strip width maximizes the flow rate. The second observation is that $Q \sim h/w$, i. e. the flow rate could be increased by using paper sheets with larger h. As thickness h is fixed from paper manufacture, the straightforward solution is parallelization: a pile of paper strips would produce an effective thickness several times larger than h.

On the other hand, the operation time is a critical aspect in these devices. In fact, for capillary-driven flows, the time to reach the strip end is $t = l_0 l/c + l^2/2c$.[19] Including l from eqn (4) yields,

$$t = \frac{l_0 w^2}{4z_C^2 sc} + \frac{w^4}{2(4z_C^2 s)^2 c}. \quad (6)$$

Once more it is found that $l_0 \to 0$ is desirable. Nevertheless, a critical feature is that the assay time grows with the fourth power of w. Therefore, diminishing the strip width has profound effects on assay time, apart from improving the throughput. One may observe that w emerges as the key geometrical factor to design diluters, concentration gradient generators, and mixers.

Optimizing the H-filter

The H-filter is an iconic microfluidic element proposed 20 years ago,[33] originally made on silicon, with open microchannels. The device has been reinvented in paper channels by the same research group.[1] The working principle of the H-filter is the difference in Brownian diffusivity among the species to be separated. As shown in Fig. 5c, the fluid stream in the left inlet arm is a solution of species A and B, with molecular diffusivities $D_0^{(A)} < D_0^{(B)}$. The diffusion zone on the right stream becomes progressively richer in the species B, which has the fastest diffusional movement. Then the species B can be selectively collected on the right outlet port. Nevertheless, if the H-filter is made on paper, the dispersivities of these chemical species under flow result, respectively:

View Article Online
DOI: 10.1039/C8AN00149A

$$D_T^{(A)} = D_0^{(A)} + sv_L, \quad (7)$$

$$D_T^{(B)} = D_0^{(B)} + sv_L. \quad (8)$$

The second term in these equations is common, since mechanical dispersion is independent of particle characteristics, as described above. Furthermore, if $v_L > v_{L,c}$, molecular diffusivity results negligible in front of the mechanical effect, and $D_T^{(A)} \approx D_T^{(B)}$. A preliminary conclusion is that paper invalidates the separation principle of the H-filter. However, one may still control the flow rate to favor the effect of Brownian diffusion.

The appropriate fluid velocity can be estimated as follows. Firstly, a minimum ratio $n = D_T^{(B)}/D_T^{(A)}$ necessary to achieve the separation has to be specified, taking into account that the concentrations of A and B at the output will differ in a factor on the order of $\exp(-n)$,[33] which is a property of the erfc function. For instance, n = 3 can produce a 20-fold enrichment of B over A. Secondly, by rationing eqn (7) and (8), the maximum fluid velocity to be used is,

$$v_{L,m} = \frac{D_0^{(B)} - nD_0^{(A)}}{s\,(n-1)}, \quad (9)$$

for a given n in the range $1 < n < D_0^{(B)}/D_0^{(A)}$. For the purposes of illustration, the following diffusion coefficients are considered: $D_0^{(B)} = 6.3\ 10^{-11}\mathrm{m}^2/\mathrm{s}$ (Blue-BSA) and $D_0^{(A)} = 6.55\ 10^{-10}\mathrm{m}^2/\mathrm{s}$ (tartrazine).[1] For n = 2, eqn (9) predicts that the maximum fluid velocity to be used in laminated W1 paper is 17 µm/s. With capillary-driven flows, the system requires a minimum upstream distance of around 6 cm, which can be provided by the length l_0 of the inlet arms. In fact, in contrast to the operations discussed above, here l_0 needs to have a minimum value. It should be pointed out that satisfying eqn (9) is critical to achieve an operative H-filter in paper format.

Conclusions

The transverse dispersion of molecules across adjacent flow streams on paper was explored by theory and experiments. Both the Brownian diffusion coefficient and the mechanical dispersion coefficient were independently measured under capillary-driven flow. To our best knowledge, it is the first time that this transport process is quantified on substrates typically used to manufacture µPADs. The most remarkable outcomes of this research are outlined as follows.

The dispersion width is independent on fluid velocity and species properties, and entirely defined by the dispersivity s. This coefficient ranges between 20 and 60 µm for laminated filter paper, being on the order of the void spaces in porous structure. From a more fundamental point of view, the relationship between s and the fiber network structure requires additional research. From a practical point of view, the magnitude of s is the essential information required for the design of operations based on transverse solute dispersion. Effectively, it was shown that the geometrical aspect ratio required for mixers, diluters, and gradient generators scales simply as $l/w \sim w/s$. Controlling the width w is also critical for the overall efficiency of these operations.

The fact that porous networks intrinsically act as mixers provides a natural advantage to µPADs: mixing and gradient formation are much more efficient on paper than in conventional microchannels. More precisely, for equal channel width, fluid velocity, and dye solution, the microchannel length needs to be D_T/D_0 times larger than the paper strip length to attain the same dispersion width. Notably, D_T/D_0 can be as large as 100, as experimentally determined.

On the other hand, it was demonstrated that the working principle of the H-filter can be hindered by mechanical dispersion, unless fluid velocity is properly handled. In fact, since molecular diffusion plays a determining role in the filtering action, separations transverse to the flow are effective only for $v_L < D_0/s$. One may finally conclude that the basic knowledge discussed throughout this work would contribute to the development of µPADs with a new level of precision and control over localized concentration profiles.

Conflicts of interest

There are no conflicts to declare.

Acknowledgements

CLAB acknowledges Dr. Federico Schaumburg for fruitful discussions on transverse dispersion, in particular on the paper-based H-filter. This research was supported by CONICET (Grant PIP-0363), ANPCyT (Grant PICT-2015-1051), and UNL (Grant CAI+D-78-5012011010010-0), Argentina.

Notes and references

1 J.L. Osborn, B. Lutz, E. Fu, P. Kauffman, D. Stevens, and P. Yager, *Lab Chip*, 2010, **10**, 2659-2665.
2 D. M. Cate, J. A. Adkins, J. Mettakoonpitak, and C. S. Henry, *Anal. Chem*., 2015, **87**, 19-41.
3 K. Yamada, H. Shibata, K. Suzuki, and D. Citterio, *Lab Chip*, 2017, **17**, 1206-1249.
4 M. M. Gong and D. Sinton, *Chem. Rev*., 2017, **117**, 8447–8480.
5 X. Wang, Z. Liu, and Y. Pang, *RSC Adv*., 2017, **7**, 29966-29984.
6 F. Deiss, A. Mazzeo, E. Hong, D. E. Ingber, R. Derda, and G. M. Whitesides, *Anal. Chem*., 2013, **85**, 8085–8094.
7 R. M. Kenney, M. W. Boyce, A. S. Truong, C. R. Bagnell, and M. R. Lockett, *Analyst*, 2016, **141**, 661-668.
8 D. I. Walsh, III, M. L. Lalli, J. M. Kassas, A. R. Asthagiri, and S. K. Murthy, *Anal. Chem*., 2015, **87**, 5505-5510.
9 B. Hong, P. Xue, Y. Wu, J. Bao, Y. J. Chuah, Y. Kang, *Biomed. Microdevices*, 2016, **18**, 21 (8pp).
10 Bear, J. *Dynamics of Fluids in Porous Media*. Elsevier Science, New York, 1972.
11 G. De Josselin de Jong, *Transactions of the American Geophysical Union*, 1958, **39**, 67-74.
12 S. T. Sie and G. W. A. Rijnders, *Anal. Chim. Acta*, 1967, **38**, 3-16.
13 S. Whitaker, *AICHE J*., 1967, **3**, 420-427.
14 B. Ph. van Milligen, P. D. Bons, *Phys Rev E*, 2012, **85**, 011306 (5pp).
15 A. Daneyko, D. Hlushkou, S. Khirevich, U. Tallarek, *J. Chromatogr. A,* 2012, **1257**, 98-155.

View Article Online
DOI: 10.1039/C8AN00149A

16 K. Smirnov and O. Shpigun, *J. Chromatogr. A*, 2015, **1375**, 27-32.
17 A. K. Yetisen, M. S. Akram and C. R. Lowe, *Lab Chip*, 2013, **13**, 2210-2251.
18 X. Jiang and Z. H. Fan, *Annu. Rev. Anal. Chem*., 2016, **9**, 203-222.
19 E. Elizalde, R. Urteaga, and C. L. A. Berli, *Lab Chip*, 2015, **15**, 2173-2180.
20 E. Fu and C. Downs, *Lab Chip*, 2017, **17**, 614-628.
21 D. M. Cate, S. D. Noblitt, J. Volckens, and C. S. Henry, *Lab Chip*, 2015, **15**, 2808-2818.
22 G. G. Morbioli, T. Mazzu-Nascimento, L. A. Milan, A. M. Stockton, and E. Carrilho, *Anal. Chem*., 2017, **89**, 4786–4792.
23 R. Ota, K. Yamada, K. Suzuki, and D. Citterio, *Analyst*, 2018, **143**, 643-653.
24 M. P. Nguyen, N. A. Meredith, S. P. Kelly, and C. S. Henry, *Anal. Chim. Acta*, 2018, **1017**, 20-25.
25 A. R. Rezk, A. Qi, J. R. Friend, W. H. Li, and L. Y. Yeo, *Lab Chip*, 2012, **12**, 773-779.
26 Crank, J. *The Mathematics of Diffusion*, Second Edition, Clarendon Press, Oxford, 1975.
27 W. Liu, C. L. Cassano, X. Xu, and Z. H. Fan, *Anal. Chem*., 2013, **85**, 10270-10276.
28 C. L. Cassano and Z. H. Fan, *Microfluid Nanofluid*, 2013, **15**, 173 (8pp).
29 E. M. Fenton, M. R. Mascarenas, G. P. López and S. S. Sibbett, *ACS Appl. Mater. Interfaces*, 2009, **1**, 124-133.
30 H. Liu, Y. Xiang, Y. Lu, and R. M. Crooks, *Angew. Chem. Int. Ed*., 2012, **51**, 6925-6933.
31 E. Elizalde, R. Urteaga, and C. L. A. Berli, *Microfluid Nanofluid*, 2016, **20**, 135 (8pp).
32 M. Mercuri, R. Gimenez, C. L. A. Berli, and M. G. Bellino, *RSC Adv.*, 2018, **8**, 6414-6418.
33 J.P. Brody and P. Yager, *Sensors and Actuators A*, 1997, **58**, 13-18.